Disentangling Electronic Spectra of Linear and Cyclic Hydrogenated Carbon Cluster Cations, C 2n+1 H + (n=3-10)

Samuel Marlton, Jack Buntine, Chang Liu, Patrick Watkins, Ugo Jacovella, Eduardo Carrascosa, James Bull, Evan Bieske

Disentangling Electronic Spectra of Linear and Cyclic Hydrogenated Carbon Cluster Cations, $C_{2n+1}H^+$ (n=3–10)

Samuel J.P. Marlton,[†] Jack T. Buntine,[†] Chang Liu,[†] Patrick Watkins,[†] Ugo Jacovella,[‡] Eduardo Carrascosa,[¶] James N. Bull,[§] and Evan J. Bieske*[,†]

†*School of Chemistry, The University of Melbourne, Victoria, Australia 3010*

‡*Université Paris-Saclay, CNRS, Institut des Sciences Moléculaires d'Orsay, 91405 Orsay, France*

¶*Bruker Daltonics GmbH & Co. KG, Fahrenheitstrasse 4, 28359 Bremen, Germany*

§*School of Chemistry, Norwich Research Park, University of East Anglia, Norwich NR4 7TJ, United Kingdom*

E-mail: evanjb@unimelb.edu.au

Abstract

Electronic spectra are measured for protonated carbon clusters ($C_{2n+1}H^+$) containing between 7 and 21 carbon atoms. Linear and cyclic $C_{2n+1}H^+$ isomers are separated and selected using a drift tube ion-mobility stage before being mass selected and introduced into a cryogenically cooled ion trap. Spectra are measured using a two-colour resonance enhanced photodissociation strategy, monitoring C_{2n+1}^+ photofragments (H atom loss channel) as a function of excitation wavelength. The linear C_7H^+, C_9H^+, $C_{11}H^+$, $C_{13}H^+$, $C_{15}H^+$ and $C_{17}H^+$ clusters, which are predicted to have polyynic structures, possess sharp $1^1\Sigma^+ \leftarrow \tilde{X}^1\Sigma^+$ transitions with well resolved vibronic progres-

sions in C-C stretch vibrational modes. The vibronic features are reproduced by spectral simulations based on vibrational frequencies and geometries calculated with time dependent density functional theory (ωB97X-D/cc-pVDZ level). The cyclic $C_{15}H^+$, $C_{17}H^+$, $C_{19}H^+$ and $C_{21}H^+$ clusters exhibit weak, broad transitions at shorter wavelength compared to their linear counterparts. Wavelengths for the origin transitions of both linear and cyclic isomers shift linearly with the number of constituent carbon atoms indicating that in both cases the clusters possess a common structural motif.

Introduction

Carbon clusters are fundamental species that are present in flames and furnaces, and in interstellar and circumstellar regions.[1,2] A characteristic feature of carbon clusters is their remarkable structural diversity, with the clusters progressively adopting linear, cyclic, bicyclic, graphene and fullerene structures with increasing cluster size.[3,4] Often there are several coexisting isomers for a particular sized cluster, presenting challenges for spectroscopic studies. Hydrogenation of carbon clusters has profound structural consequences; addition of one or two H atoms to small carbon clusters favours linear structures, delays the onset for the formation of monocyclic rings, and suppresses formation of fullerenes.[5,6] Despite the intriguing issues surrounding the formation, structures, and properties of small hydrogenated carbon clusters there have been relatively few spectroscopic studies.

In this paper we present and discuss electronic spectra of protonated carbon clusters containing between 7 and 21 carbon atoms. Although an electronic spectrum has been measured for C_5H^+ trapped in a neon matrix,[7] to our knowledge there are no previously reported electronic spectra for larger $C_{2n+1}H^+$ clusters. The $C_{2n+1}H^+$ clusters discussed in this paper span a size range over which they are expected to go from possessing linear structures to adopting cyclic structures such that for certain sizes linear and cyclic isomers coexist.[6] To deal with this potential ambiguity we have adopted an experimental approach whereby the target isomer population is selected according to the ions' collision cross section (CCS) with

He buffer gas prior to mass selection and spectroscopic interrogation in a cryogenically cooled quadrupole ion trap. We have recently used this isomer-selective scheme to obtain electronic spectra of monocyclic C_{2n}^+ clusters over the n=6–14 range.[8,9]

Small linear C_nH^+ clusters are known to exist in extraterrestrial environments, with C_3H^+ and C_5H^+recently discovered in the interstellar medium (ISM) through their microwave transitions.[10–12] The C_7H^+ cluster is predicted to exist in even greater abundance than C_3H^+.[12] Related neutrals C_3H, C_4H,[13] C_5H,[14,15] C_6H,[16,17] C_7H,[18] and C_8H,[19] and anions C_4H^-,[20] C_6H^-,[21] and C_8H^-[22] have also been detected in extraterrestrial regions. Progress in the spectroscopic characterization of related carbon species is described in several reviews.[23–26] Electronic spectra have been obtained for linear neutral C_nH clusters containing up to 16 carbon atoms,[27] and linear anion C_nH^- clusters with up to 24 carbon atoms.[24,28] Anion C_nH^- (n=2-9) clusters have also been characterized using photoelectron spectroscopy to provide information on the neutral C_nH molecules.[29,30] The singly hydrogenated carbon clusters characterized spectroscopically so far have been linear. Here, for the first time we present electronic spectra for singly hydrogenated carbon clusters with cyclic structures, representing a first step towards generating and spectroscopically characterizing more structurally complex hydrocarbon species from the bottom up.

Experimental Details

The experimental apparatus has been described previously, with a comprehensive description available in ref. 9. Briefly, protonated carbon clusters (C_nH^+) were generated by ablating the surface of a rotating graphite disk using the output of a pulsed Nd:YAG laser (λ=532 nm, 14 mJ/pulse, 100 Hz). The ions were propelled by an electric field through a drift region where they were separated spatially and temporally according to their collision cross sections with He buffer gas (P≈2 Torr). Following the drift region the ion packet was compressed radially using an RF ion funnel and passed through a 1.0 mm orifice into an RF hexapole ion guide in

a differentially pumped region. From there the ions passed through a quadrupole mass filter (QMF) where they were mass selected. For recording arrival time distributions (ATDs), the ions were then deflected 90° to an off-axis ion detector connected to a multichannel scaler.

For the spectroscopy experiments, an electrostatic Bradbury-Nielsen ion gate located at the end of the drift region was opened at an appropriate time and duration to allow passage of either the linear or cyclic $C_{2n+1}H^+$ isomer population. Mobility-selected ions generated from 50 shots of the ablation laser were stored in the hexapole ion guide and were then ejected into the QMF where they were mass selected. The ions then passed through an octupole ion guide into a three-dimensional quadrupole ion trap (QIT) mounted on a cryohead ($T \approx 10$ K), where they were collisionally cooled by He gas injected through a pulsed valve into the trap at 2 Hz.

Electronic spectra of the $C_{2n+1}H^+$ clusters were recorded using two-colour resonance-enhanced photodissociation scheme monitoring C_{2n+1}^+ photofragments (H atom loss channel). In alternate trapping cycles, after 400 ms the ion packet in the QIT was exposed to a single pulse from a tunable optical parametric oscillator (OPO, EKSPLA NT342B, 6 ns pulse width, bandwidth $\approx 4\,cm^{-1}$). For the linear clusters the pulse energy was $\leq 50\,\mu J/cm^2$/pulse, whereas for the cyclic clusters it was $\leq 500\,\mu J/cm^2$/pulse. The first OPO pulse was followed 10 ns later by a single shot from a Nd:YAG laser (λ=532 nm, pulse energy $\approx 2\,mJ/cm^2$/pulse) to provide sufficient energy to photodissociate the C_nH^+ clusters (H atom loss). The pulse energies for the tunable laser beam and 532 nm beam were reduced to a level where both beams were required to cause photodissociation when the tunable beam was tuned to a resonance. Therefore it is unlikely that the clusters absorbed more than a single photon from the tunable beam. According to DFT ωB97X-D/cc-pVDZ calculations, absorption of a single additional 532 nm photon should be sufficient to dissociate the linear C_7H^+ and C_9H^+ clusters, whereas the larger linear clusters probably require two additional 532 nm photons (Figure S1 in the SI). The cyclic clusters should require only a single additional 532 nm photon to photodissociate (Figure S1 in the SI). Generally, the photodissociation yield was

insensitive to the time delay between the first and second light pulses over a 0-1 μs range leading us to suspect that resonant excitation to a higher electronic state by the first OPO pulse was followed by internal conversion to highly excited vibrational levels in the ground electronic state before arrival of the 532 nm light pulse.The ions were ejected from the QIT after 480 ms into a linear time-of-flight mass spectrometer (ToFMS). The electronic spectrum was obtained by monitoring the C_{2n+1}^+ photofragment signal (laser-on minus laser-off signal) as a function of OPO wavelength.

The protonated carbon clusters were generated by the laser ablation ion source along with far larger populations of pure carbon cluster cations. We presume that the hydrogen source was trace water vapour in the He buffer gas. The fact that the protonated carbon clusters are associated with sharp peaks in the ATD (Figure 1) proves that they are formed in the laser ablation ion source rather than from C_n^+ clusters reacting with H_2O or some other impurity in the drift region, or even further downstream in the instrument. In future, the formation mechanism could perhaps be explored by soaking the graphite disk in D_2O.

Computational Details

Geometries for $C_{2n+1}H^+$ clusters in their ground and excited electronic states were optimised using density functional theory (DFT) and time-dependent density functional theory (TD-DFT) employing the ωB97X-D functional.[31] The optimised ωB97X-D geometries were used for all other calculations. Vibrational frequencies were calculated to confirm that the geometries correspond to minima by the absence of imaginary vibrational frequencies and to provide vibrational zero-point energy corrections. Ground state electronic energies for cyclic clusters were recalculated using coupled cluster singles and doubles (CCSD) and excited state electronic energies were recalculated using equation of motion coupled cluster singles and doubles (EOM-CCSD). The ground state electronic energies of all clusters were recalculated using the domain-based local pair natural orbital coupled cluster method with singles doubles and perturbative triples (DLPNO-CCSD(T))[32,33] using restricted open-shell

Hartree-Fock reference wavefunctions.[34] DLPNO-CCSD(T) calculations were undertaken using the ORCA/4.2.1 software.[35,36] The DFT, TDDFT, CCSD and EOM-CCSD calculations were undertaken using the Gaussian16 software.[37] All calculations employed the cc-pVDZ basis set,[38,39] except the DLPNO-CCSD(T) calculations, which employed the TZVP basis set.[40] The vibronic structure of the electronic transitions were simulated using the PGOPHER software.[41]

Results and Discussion

Linear and cyclic structures for $C_{2n+1}H^+$ clusters

We begin by discussing the ion mobility data, which provide evidence for the existence of linear and cyclic $C_{2n+1}H^+$ clusters. ATDs for protonated carbon clusters (C_7H^+ to $C_{21}H^+$) are shown in Figure 1. In each trace, there is a fast peak and a slow peak that can be assigned to cyclic and linear C_nH^+ isomers, respectively. The cyclic clusters are more compact and have smaller collision cross sections than the linear clusters and pass more quickly through the He buffer gas in the drift region (see ref. 9). The peak assignments are supported by collision cross section calculations, which predict that CCSs for linear clusters should be 15-20% larger than CCSs for cyclic clusters (see Table S1 in the SI) consistent with the ATD data. Note that the relative populations of the linear and cyclic $C_{2n+1}H^+$ isomers cannot easily be determined from the ATD peak intensities in Figure 1 because the $C_{2n+1}H^+$ clusters have the same m/z and similar arrival times as C^+_{2n+1} clusters containing a single ^{13}C atom. This may be part of the reason that for $C_{11}H^+$ and larger clusters the cyclic ATD peaks in Figure 1 are broader than the linear peaks. Nevertheless, it is clear from Figure 1 that linear clusters are more stable than cyclic clusters for C_7H^+ and C_9H^+, and that cyclic clusters progressively become the dominant form with increasing size, such that for $C_{21}H^+$ there is almost no trace of the linear isomer. These results are broadly consistent with the observations of Bowers and co-workers for hydrogenated carbon clusters generated by

laser ablation of graphite surrounded by a 10% H_2/90% He gas mixture, with cyclic clusters progressively supplanting linear clusters over the C_9H^+ to $C_{15}H^+$ range.[6]

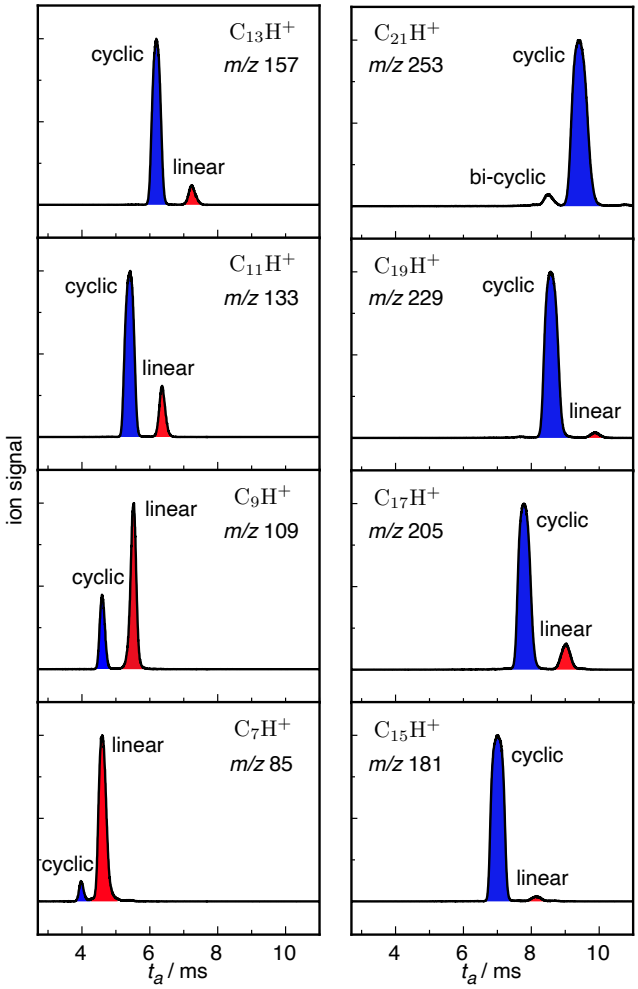

Figure 1: Arrival time distributions (ATDs) for $C_{2n+1}H^+$ clusters propelled by an electric field through He buffer gas. The two peaks in each trace correspond to linear (red) and cyclic (blue) $C_{2n+1}H^+$ isomers. Note that in each case, the isomer peak contains a contribution from the C^+_{2n+1} cluster containing a single ^{13}C atom. The ATD for $C_{21}H^+$ also contains a small peak at short arrival time (t_a≈8.5 ms) that is probably due either to a protonated bicyclic isomer or to a bicyclic isomer of C^+_{21} containing one ^{13}C atom. Electronic spectra shown in Figure 3 and Figure 6 were taken by selecting, trapping, and probing linear and cyclic $C_{2n+1}H^+$ isomers, respectively.

The structures of linear $C_{2n+1}H^+$ clusters and two possible cyclic $C_{2n+1}H^+$ isomers are shown in Figure 2. Relative energies for the isomers calculated at the DLPNO-CCSD(T)/TZVP level are plotted in Figure 2D with geometries and zero-point energy corrections calculated

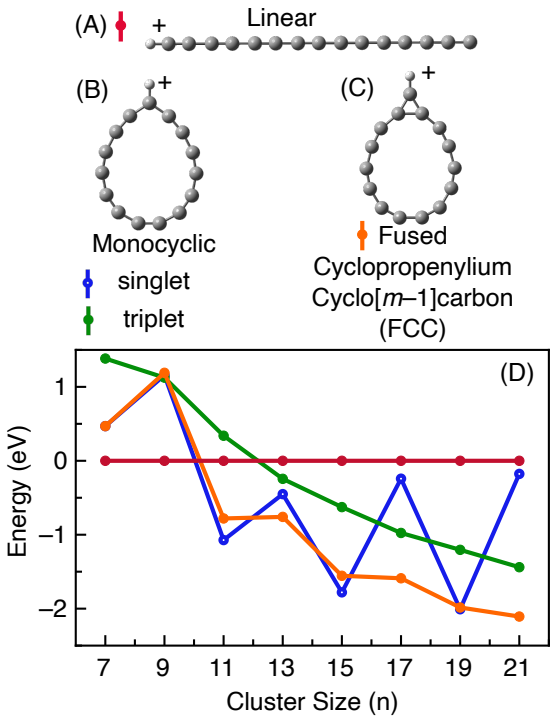

Figure 2: Linear (A), monocyclic (B) and FCC (C) isomers for $C_{2n+1}H^+$ clusters. Energies for the isomers with respect to the energy of the linear isomer are plotted in D. Electronic energies are calculated at the DLPNO-CCSD(T)/TZVP level using geometries and zero-point energy corrections calculated at the DFT ωB97X-D/cc-pVDZ level.

at the DFT ωB97X-D/cc-pVDZ level. All clusters are predicted to possess polyynic structures with pronounced bond length alternation (see Figures S2-S7 in the SI). One plausible structure for cyclic $C_{2n+1}H^+$ clusters is a monocyclic carbon ring with an attached hydrogen atom lying outside the ring – essentially a tadpole structure with the hydrogen atom as the tail (Figure 2B). The ground electronic state for the monocyclic structure is predicted to have singlet multiplicity for $C_{15}H^+$ and $C_{19}H^+$, and triplet multiplicity for $C_{17}H^+$ and $C_{21}H^+$. Another plausible isomer for cyclic $C_{2n+1}H^+$ clusters consists of a cyclopropenium ring fused to a larger carbon ring (Figure 2C). Henceforth, this structure is referred to as FCC, denoting fused cyclopropenylium cyclo[m–1]carbon, where m is the number of carbon atoms in the molecule. Only singlet states were considered for FCC structures because in each case the lowest energy triplet state lies at least 1 eV higher in energy.

For $C_{15}H^+$ and $C_{19}H^+$ the monocyclic singlet tadpole structure is predicted to lie slightly

lower in energy, whereas for $C_{17}H^+$ and $C_{21}H^+$ the FCC structure is predicted to be more stable. Although the lower energy isomer might be expected to be more abundant, it is possible that higher energy isomers are present if they are produced efficiently in the ion source and are separated from the most stable form by a substantial energy barrier.

The linear isomer is more stable than the monocyclic and FCC isomers for C_7H^+ and C_9H^+, consistent with the greater intensity of the linear isomer peak compared to the cyclic isomer peak in the C_7H^+ and C_9H^+ ATDs shown in Figure 1. With increasing size, the monocyclic and FCC isomers are predicted to become more stable than the linear isomer (Figure 2D), in line with the decreasing intensity of the linear isomer ATD peak and its eventual disappearance at $C_{21}H^+$ (see Figure 1). Although the ATDs provide an indication of the relative abundances for the linear and cyclic isomers, they are less useful for distinguishing between the monocyclic and FCC isomers, which are predicted to have CCSs that differ by less than 2% (see Table S1 in the SI).

Electronic spectra of $C_{2n+1}H^+$ clusters

Linear clusters

We first consider electronic spectra of the linear C_7H^+, C_9H^+, $C_{11}H^+$, $C_{13}H^+$, $C_{15}H^+$ and $C_{17}H^+$ clusters shown in Figures 3 & 4. Band wavenumbers and assignments are provided in Table S2 & S3 in the SI. The spectra are all similar in appearance, each displaying sharp peaks arranged in two prominent vibronic progressions suggesting that the clusters share a common structural motif. Wavelengths for the origin transitions depend linearly on the number of constituent carbon atoms (Figure 5), establishing a trend, which, when extrapolated, fits with the origin transition of linear C_5H^+ (250.1 nm), whose spectrum has been measured in a neon matrix.[7] There is a strong correlation between the calculated adiabatic transition energies for the linear $C_{2n+1}H^+$ (n=3–8) clusters and the measured origin transition energies, albeit with a constant energy offset (see Figure S8 in the SI). On the basis of the excited state calculations and the previous C_5H^+ matrix investigation,[7] the observed band systems

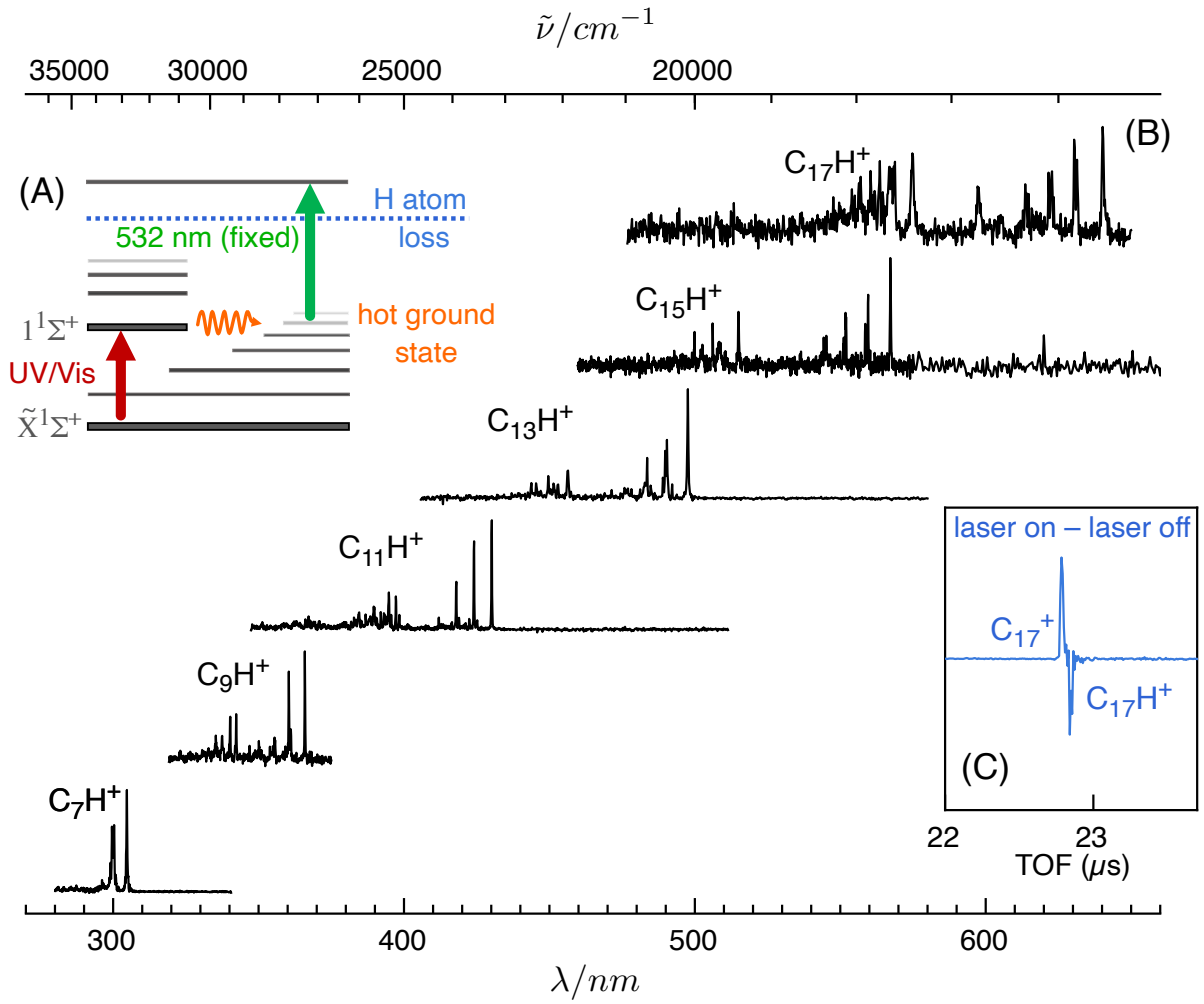

Figure 3: (A) 2-colour scheme for obtaining spectra of $C_{2n+1}H^+$ clusters. The second fixed-wavelength 532 nm light pulse was delayed by 10 ns with respect to the first tunable light pulse from the OPO. (B) The $1^1\Sigma^+ \leftarrow \tilde{X}^1\Sigma^+$ electronic spectra for linear $C_{2n+1}H^+$ clusters obtained by monitoring C_{2n+1}^+ photofragments (H atom loss channel) as a function of OPO wavelength. (C) Difference between laser-on and laser-off ToF signal for $C_{17}H^+$ with the wavelength for the light tuned to the origin transition.

are assigned to $1^1\Sigma^+ \leftarrow \tilde{X}^1\Sigma^+$ electronic transitions, which are predicted to have very large oscillator strengths (f=2.6 for C_7H^+, f=3.3 for C_9H^+, f=3.9 for $C_{11}H^+$, f=4.5 for $C_{13}H^+$, f=4.9 for $C_{15}H^+$, and f=5.2 for $C_{17}H^+$ based on ωB97X-D/cc-pVDZ TDDFT level calculations). The large oscillator strengths are consistent with our observation that it was easy to saturate the transitions such that it was necessary to severely attenuate the tunable OPO beam to avoid power broadening the bands. The TD-DFT ωB97X-D/cc-pVDZ calculations overestimate the measured origin transition energies by $\approx$1 eV, whereas the EOM-CCSD/cc-

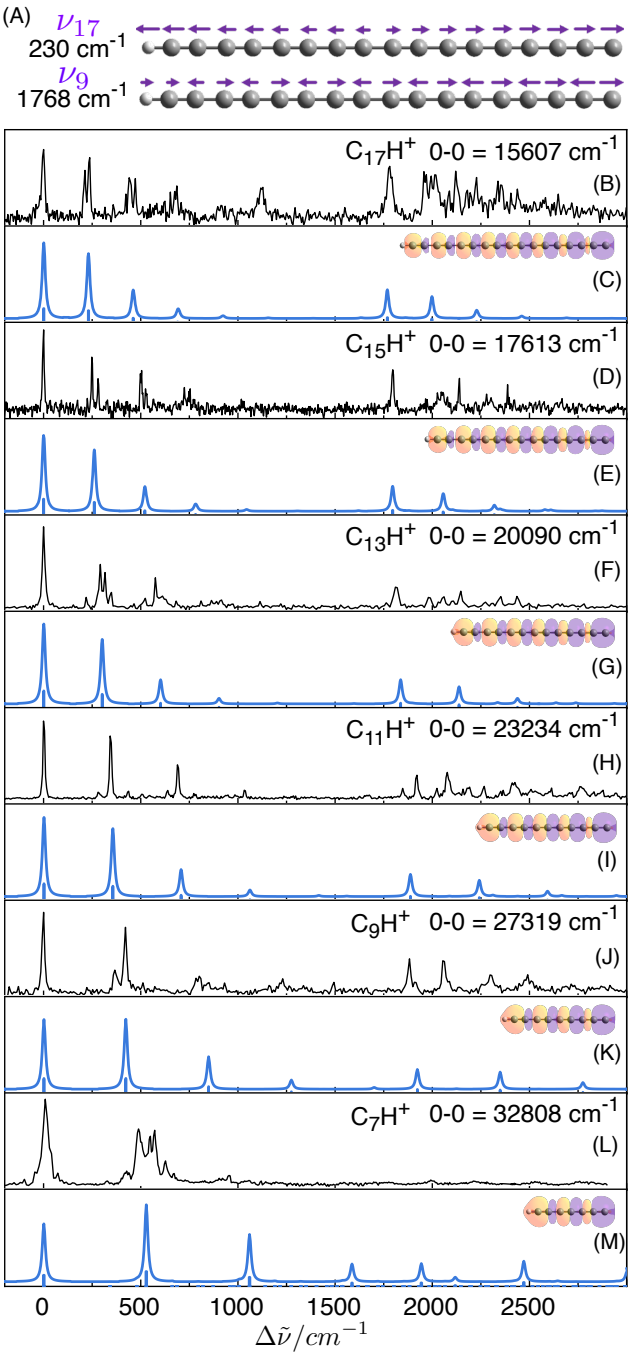

Figure 4: (A) The two σ progression-forming vibrational modes for $1^1\Sigma^+ \leftarrow \tilde{X}^1\Sigma^+$ band systems of linear $C_{2n+1}H^+$ clusters. (B–M) Experimental $1^1\Sigma^+ \leftarrow \tilde{X}^1\Sigma^+$ spectra for linear $C_{2n+1}H^+$ clusters (black traces) compared to Franck-Condon simulations (blue traces). Vibrational frequencies and bond lengths are calculated at the TD-DFT ωB97X-D/cc-pVDZ level. Calculated frequencies are unscaled in the simulations. The transition density is presented above each simulated spectrum. The simulated spectra are offset by $\approx$1 eV to align with the experimental spectra (see Table S3 in the SI).

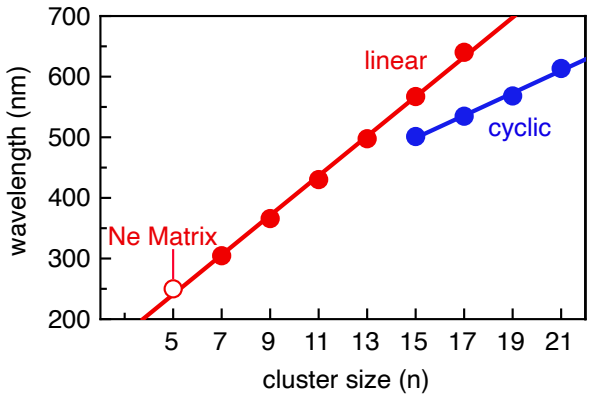

Figure 5: Measured 0_0^0 transition wavelengths for linear (red) and cyclic (blue) $C_{2n+1}H^+$ clusters plotted as a function of cluster size. The $1^1\Sigma^+ \leftarrow \tilde{X}^1\Sigma^+$ transition wavelength for linear C_5H^+ measured in a Ne matrix from ref. 7 is shown as an open circle. Other data are from the current work.

pVDZ calculations (with ωB97X-D/cc-pVDZ geometries and ZPE corrections) overestimate the measured origin transition energies by $\approx$0.7 eV (see Figure S8 in the SI).

The $1^1\Sigma^+ \leftarrow \tilde{X}^1\Sigma^+$ band systems of the linear $C_{2n+1}H^+$ clusters are dominated by two vibronic progressions involving totally symmetric (σ) C-C stretching modes. The first Franck-Condon active mode corresponds to the lowest frequency C-C stretch mode ν_m, where m is the number of carbon atoms in the cluster. The measured frequency for this vibrational mode decreases from 480 cm^{-1} for C_7H^+ to 237 cm^{-1} for $C_{17}H^+$. The other Franck-Condon active vibrational mode corresponds to a higher frequency C-C stretch mode $\nu_{(m+1)/2}$ whose measured frequency decreases from 1982 cm^{-1} for C_7H^+ to 1781 cm^{-1} for $C_{17}H^+$. The natures of these two vibrational modes are illustrated for $C_{17}H^+$ in Figure 4A. As shown in Figure 4(B-M), the simulated spectra calculated using Franck-Condon factors based on ground and excited state geometries and vibrational frequencies, adequately reproduce the experimental spectra.

The experimental spectra exhibit additional vibronic bands that are not predicted by the Franck-Condon simulations, and which are presumably associated with transitions to bending overtone states that gain intensity through Fermi resonance with the σ stretch states. Ultimately, explanation and assignment for these peaks will require higher resolution

spectra and more sophisticated calculations that consider anharmonicity and mixing of the excited state bending and stretching vibrational modes.

Cyclic $C_{2n+1}H^+$ clusters

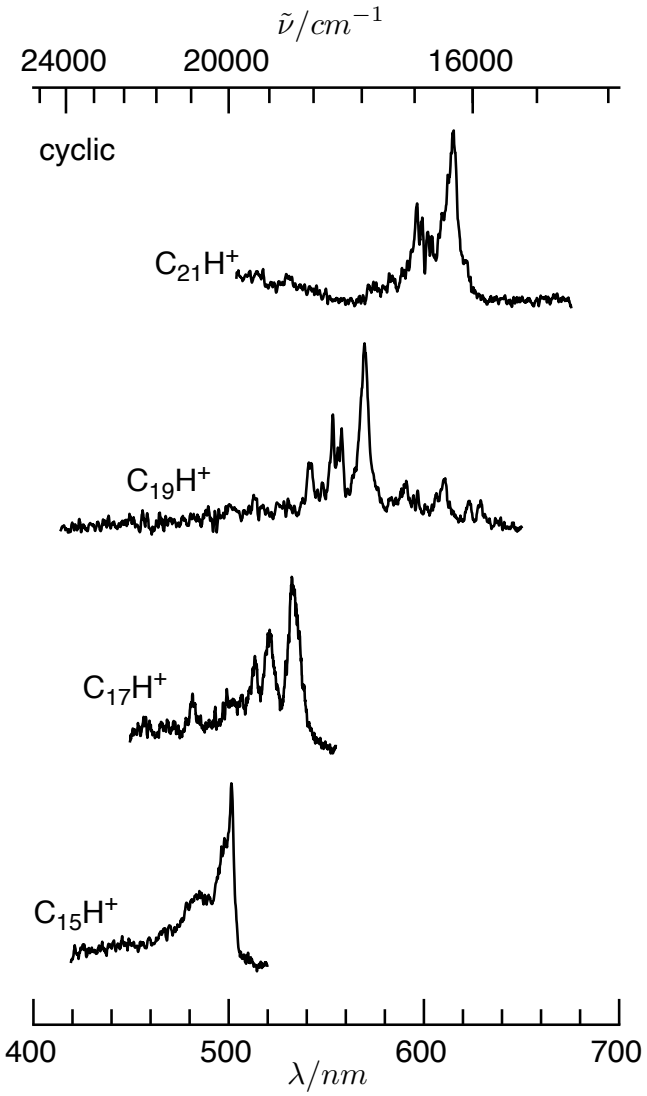

Figure 6: Electronic spectra for cyclic $C_{2n+1}H^+$ clusters obtained by monitoring C^+_{2n+1} photofragments (H loss channel) as a function of OPO wavelength.

We now consider the electronic spectra of the cyclic $C_{15}H^+$, $C_{17}H^+$, $C_{19}H^+$, $C_{21}H^+$ clusters shown in Figure 6. Band wavenumbers and assignments are provided in Table S4 in the SI. Generally the spectra are similar to one another, with each exhibiting a relatively broad origin band flanked by a series of bands with diminishing intensity extending to higher

energy. The first of these peaks is spaced by 350–600 cm^{-1} from the origin transition. There is a linear dependence of the wavelength for the origin bands on the number of carbon atoms in the clusters (see Figure 5), suggesting that the spectra arise from $C_{2n+1}H^+$ clusters with a common structural motif. Interestingly, the $C_{19}H^+$ spectrum exhibits several weaker peaks to the red of the main band system, which may be associated with another band system. No corresponding peaks were found for the $C_{15}H^+$, $C_{17}H^+$, and $C_{21}H^+$ clusters.

Analysis of the cyclic isomer spectra is complicated by several factors. First, the transitions are relatively broad and weak compared to the transitions of the corresponding linear clusters. Second, there are two predicted cyclic isomers – monocyclic and FCC forms (Figure 2B, C) – either or both of which are conceivably produced by the ion source. The two isomers are predicted to have CCSs differing by less than 2% and are probably not distinguishable or separable using the ion mobility stage of the instrument. Third, conducting excited state calculations for the cyclic clusters is challenging and the results are of uncertain reliability, especially considering that even the ground state of neutral carbon rings are notoriously difficult to describe computationally.[42–46]

We first consider the possibility that the $C_{15}H^+$, $C_{17}H^+$, $C_{19}H^+$, $C_{21}H^+$ clusters all have monocyclic structures. Although, FCC structures are predicted to be more stable than monocyclic structures for $C_{17}H^+$ and $C_{21}H^+$ (Figure 2D) it is possible that the monocyclic isomers are formed efficiently in the ion source and that substantial barriers prevent conversion to the FCC isomer. Based on calculated energies shown in Figure 2, the ground states of $C_{15}H^+$ and $C_{19}H^+$ should have singlet multiplicity, whereas the ground states of $C_{17}H^+$ and $C_{21}H^+$ should have triplet multiplicity. For $C_{15}H^+$ and $C_{19}H^+$, the EOM-CCSD/cc-pVDZ calculations predict a pair of singlet-singlet electronic transitions occurring within 0.2–0.3 eV of the observed transitions (see Figure S9 and Table S5 in the SI). Attempts to calculate the excited states of the triplet $C_{17}H^+$ and $C_{21}H^+$ cyclic clusters with EOM-CCSD were frustrated by spin contamination, with $\langle S^2 \rangle = 4.67$ for the UHF reference wavefunction of $C_{17}H^+$ and $\langle S^2 \rangle = 6.61$ for that of $C_{21}H^+$ ($\langle S^2 \rangle$ should be 2.00 for a triplet). Although we

were unable to calculate reliable triplet-triplet transition energies, the singlet-singlet transitions for $C_{11}H^+$, $C_{15}H^+$ and $C_{19}H^+$ are predicted to progressively shift to lower energy with increasing number of constituent carbon atoms as observed experimentally.

It is also possible that FCC isomers are formed efficiently in the ion source. Predicted vertical transitions for the singlet FCC clusters are in the 350–450 nm range and are shifted to higher energy from the observed transitions of the cyclic clusters by 0.5–0.9 eV. Transition wavelengths for the FCC clusters are not predicted to change significantly with cluster size (Figure S9 in the SI). This is at odds with the observed progressive shift to longer wavelength of the transitions for $C_{15}{}^+$ to $C_{21}{}^+$. In summary, the exact structures of the cyclic $C_{2n+1}H^+$ clusters and the nature of their electronic absorptions remain unclear. The spectra shown in Figure 6 could arise from monocyclic structures, FCC structures, or some combination of both. Distinguishing between the different cyclic isomers will require reliable excited state calculations, and perhaps spectra obtained in other ranges, including the infrared.

Astrophysical Considerations

The protonated carbon clusters investigated in the current study may exist in extraterrestrial and interstellar environments, particularly given that the smaller C_3H^+ and C_5H^+ species have already been detected in the interstellar medium through their rotational transitions,[11,12] as have the related neutral species C_4H to C_8H,[13–19] and anions C_4H^-,C_6H^- and C_8H^-.[20–22]

All of the $C_{2n+1}H^+$ clusters have non-zero dipole moment and are in principle detectable through their microwave transitions. Dipole moments calculated as part of the DLPNO-CCSD(T) method for different $C_{2n+1}H^+$ isomers are listed in Table 1, and for the linear isomers are given along with charge distributions calculated using CCSD/cc-pVDZ in Figure S10 in the SI. Interestingly, the magnitude of the dipole moment for the linear clusters decreases from C_7H^+ to $C_{11}H^+$ and thereafter increases. For cyclic structures, the dipole moment increases with cluster size, with the FCC isomer of $C_{21}H^+$ having the largest predicted

dipole moment (11.2 D) of all the studied species.

The linear $C_{11}H^+$, $C_{13}H^+$, $C_{15}H^+$ and $C_{17}H^+$ clusters exhibit very strong electronic transitions over the 400–700 nm range so it is worth briefly considering whether they could be responsible for any diffuse interstellar bands (DIBs). The origin transitions of linear $C_{11}H^+$, $C_{13}H^+$, $C_{15}H^+$ and $C_{17}H^+$ occur at 430.3, 497.6, 567.6, and 640.6 nm, respectively, none of which correspond to DIBs observed for HD204827 or HD183143.[47,48] Furthermore, the linear clusters exhibit pronounced vibronic progressions, at odds with the absence of correlations between the intensities of different DIBs observed along various sight lines. Therefore, we conclude that it is unlikely that linear $C_{2n+1}H^+$ clusters are DIB carriers for these clouds. The absence of the origin transitions for $C_{11}H^+$, $C_{13}H^+$, $C_{15}H^+$ and $C_{17}H^+$ in reported spectra of HD 183143,[48] allows us to estimate maximum column densities as 0.7-1.3$\times10^{11}$ cm^{-2} (see Section S7 in the SI). Nevertheless, the electronic spectra presented here could be used for more thorough comparisons with other DIB databases that consider different lines of sight and clouds with different densities and chemical conditions.

Previous investigations show that PAH cations contained in ion traps exposed to intense bursts of laser light eventually decompose to form bare carbon cluster cations (C_n^+), through loss of H, H_2 and small hydrocarbon molecules.[49–52] Similar photofragmentation processes are postulated to occur in interstellar space driven by the flux of harsh UV radiation. The $C_{2n+1}H^+$ species examined in the current work can be viewed as the penultimate species in this dehydrogenation process. Although, the stoichiometric formulae of the intermediates and products are derived in the ion trap experiments, the actual structures of the chemical species are unknown. Here we have demonstrated that different $C_{2n+1}H^+$ isomers can be distinguished through their drift mobilities and their electronic spectra, laying foundation for future measurements in which the final stages of PAH^+ photodecomposition are explored with isomer specificity.

Table 1: Dipole moments (in Debye) for $C_{2n+1}H^+$ clusters calculated as part of the DLPNO-CCSD(T)/TZVP method using ωB97X-D/cc-pVDZ optimised geometries.

	linear	monocycle singlet	monocycle triplet	FCC
C_7H^+	2.7	2.7	1.2	2.7
C_9H^+	1.8	3.4	1.5	5.8
$C_{11}H^+$	0.4	3.1	1.6	4.8
$C_{13}H^+$	1.7	4.4	1.9	6.2
$C_{15}H^+$	4.3	4.0	0.3	6.6
$C_{17}H^+$	7.4	3.1	0.0	8.5
$C_{19}H^+$	11.2	6.3	0.9	9.3
$C_{21}H^+$	15.4	4.8	1.6	11.2

Conclusions and Outlook

Electronic spectra of cryogenically cooled linear and cyclic $C_{2n+1}H^+$ clusters have been measured using two-colour REPD spectroscopy. A key feature of the experimental approach is the separation and selection of linear and cyclic isomers prior to trapping and spectroscopic interrogation. Ion mobility measurements show that clusters smaller than $C_{13}H^+$ prefer linear structures with cyclic clusters becoming the dominant species for clusters larger than $C_{15}H^+$. Spectra were acquired for linear isomers with $7 \leq 2n+1 \leq 17$ and for cyclic isomers with $15 \leq 2n+1 \leq 21$. Isomer selection prior to spectroscopic interrogation was particularly useful for $C_{15}H^+$ and $C_{17}H^+$ for which the linear and cyclic isomers coexist. The linear isomers exhibit strong $1^1\Sigma^+ \leftarrow \tilde{X}^1\Sigma^+$ band systems with sharp vibronic features and origin transitions whose wavelengths shift linearly with the number of constituent carbon atoms. In comparison, the cyclic isomers have weaker bands systems occurring at shorter wavelength, and much broader transitions. Together, the experimental and theoretical data provide foundations for better understanding the structures, photostabilities, and electronic transitions of astrophysically relevant $C_{2n+1}H^+$ clusters.

There are several avenues to extend the current work. First, it would be interesting to measure electronic spectra for cyclic $C_{2n+1}H^+$ clusters larger than $C_{21}H^+$ to explore whether their electronic spectra continue to evolve in a systematic fashion with increasing size. This

may help resolve whether the cyclic clusters prefer monocyclic or FCC structures. Second, characterizing the $C_{2n+1}H^+$ clusters in other spectral ranges, including the microwave region, is desirable given their large dipole moments and possible astrophysical relevance. Infrared studies would also provide more information on the evolution of cluster structures and vibrational frequencies with size.[25] More generally, the ion mobility strategy employed in the current study should be useful for characterizing related hydrogenated carbon clusters that also possess several isomers. For example, $C_{2n}H^-$ anion clusters with n=5–12 exhibit two series of electronic absorptions whose relative intensities depend on ion source conditions, and which presumably arise from different isomers.[27] The experimental approach employed in the present study may help elucidate the nature of these co-existing species.

Finally, we note that photodissociation of linear $C_{2n+1}H^+$ clusters (H loss) may provide a means to generate linear carbon clusters (C^+_{2n+1}) over a size range where the cyclic isomer is produced almost exclusively by usual ion sources. In principle, following their creation through photodissociation and cooling in a cryogenic ion trap, the photofragment C^+_{2n+1} clusters could be probed using laser-based action spectroscopy techniques to extend the range of spectroscopically characterized carbonaceous species.

Supporting Information Available

The Supporting Information contains calculated dissociation energies, measured and calculated collision cross sections for $C_{2n+1}H^+$ clusters, experimental and calculated transition wavelengths, calculated bond lengths for linear and cyclic structures, electrostatic potentials for linear clusters, calculated vibrational frequencies for linear $C_{2n+1}H^+$ clusters in the ground and excited states, and Cartesian coordinates for the DFT ωB97X-D optimised geometries.

Acknowledgement

This research was supported under the Australian Research Council's Discovery Project

funding scheme (Project Numbers DP150101427 and DP160100474). U. Jacovella and J. Buntine acknowledge support from the Swiss National Science Foundation (P2EZP2_178429) and the Australian Research Training Program scheme, respectively. The authors thank Richard Mathys of the Science Faculty Workshop for his indispensable contributions to the design and construction of the apparatus used in this study.

Conflict of Interest

The authors have no conflicts to disclose.

Data Availability Statement

The data that support the findings of this study are available from the corresponding author upon reasonable request.

References

(1) Weltner, W.; Van Zee, R. J. Carbon molecules, ions, and clusters. *Chem. Rev.* **1989**, *89*, 1713–1747.

(2) Van Orden, A.; Saykally, R. J. Small carbon clusters: Spectroscopy, structure, and energetics. *Chem. Rev.* **1998**, *98*, 2313–2357.

(3) Kroto, H. W.; Heath, J. R.; O'Brien, S. C.; Curl, R. F.; Smalley, R. E. C_{60}: Buckminsterfullerene. *Nature* **1985**, *318*, 162–163.

(4) von Helden, G.; Hsu, M. T.; Gotts, N.; Bowers, M. T. Carbon cluster cations with up to 84 atoms: structures, formation mechanism, and reactivity. *J. Phys. Chem.* **1993**, *97*, 8182–8192.

(5) Heath, J. R.; Zhang, Q.; O'Brien, S. C.; Curl, R. F.; Kroto, H. W.; Smalley, R. E. The formation of long carbon chain molecules during laser vaporization of graphite. *J. Am. Chem. Soc.* **2002**, *109*, 359–363.

(6) Lee, S.; Gotts, N.; von Helden, G.; Bowers, M. T. Structures of $C_nH_x^+$ molecules for $n \leq 22$ and $x \leq 5$: Emergence of PAHs and effects of dangling bonds on conformation. *J. Phys. Chem. A* **1997**, *101*, 2096–2102.

(7) Fulara, J.; Nagy, A.; Chakraborty, A.; Maier, J. P. Electronic transitions of C_5H^+ and C_5H: Neon matrix and CASPT2 studies. *J. Chem. Phys.* **2016**, *144*, 244309.

(8) Buntine, J. T.; Cotter, M. I.; Jacovella, U.; Liu, C.; Watkins, P.; Carrascosa, E.; Bull, J. N.; Weston, L.; Muller, G.; Scholz, M. S. et al. Electronic spectra of positively charged carbon clusters - $C_{2n}^+(n=6–14)$. *J. Chem. Phys.* **2021**, *155*, 214302.

(9) Buntine, J. T.; Carrascosa, E.; Bull, J. N.; Jacovella, U.; Cotter, M. I.; Watkins, P.; Liu, C.; ; Scholz, M. S.; Adamson, B. D. et al. An ion mobility mass spectrometer coupled with a cryogenic ion trap for recording electronic spectra of charged, isomer-selected clusters. *Rev. Sci. Instrum.* **2022**, *93*, 043201.

(10) Pety, J.; Gratier, P.; Guzmán, V.; Roueff, E.; Gerin, M.; Goicoechea, J. R.; Bardeau, S.; Sievers, A.; Le Petit, F.; Le Bourlot, J. et al. The IRAM-30 m line survey of the Horsehead PDR - II. First detection of the l-C_3H^+ hydrocarbon cation. *Astron. Astrophys.* **2012**, *548*, A68.

(11) Brünken, S.; Kluge, L.; Stoffels, A.; Asvany, O.; Schlemmer, S. Laboratory rotational spectrum of l-C_3H^+ and confirmation of its astronomical detection. *Astrophys. J. Lett.* **2014**, *783*, L4.

(12) Cernicharo, J.; Agúndez, M.; Cabezas, C.; Fuentetaja, R.; Tercero, B.; Marcelino, N.; Endo, Y.; Pardo, J.; de Vicente, P. Discovery of C_5H^+ and detection of C_3H^+ in TMC-1 with the QUIJOTE line survey. *Astron. Astrophys.* **2022**, *657*, L16.

(13) Guélin, M.; Green, S.; Thaddeus, P. Detection of the C_4H radical toward IRC plus 10216. *Astrophys. J.* **1978**, *224*, L27–L30.

(14) Cernicharo, J.; Kahane, C.; Gomez-Gonzalez, J.; Guélin, M. Detection of the $^2\Pi_{3/2}$ state of C_5H. *Astron. Astrophys.* **1986**, *167*, L5–L7.

(15) Cernicharo, J.; Guélin, M.; Walmsley, C. Detection of the hyperfine structure of the C_5H radical. *Astron. Astrophys.* **1987**, *172*, L5.

(16) Suzuki, H.; Ohishi, M.; Kaifu, N.; Ishikawa, S.-I.; Kasuga, T. Detection of the interstellar C_6H radical. *Publ. Astron. Soc. Jpn.* **1986**, *38*, 911–917.

(17) Guélin, M.; Cernicharo, J.; Kahane, C.; Gomez-Gonzalez, J.; Walmsley, C. Detection of a heavy radical in IRC+ 10216: The hexatriynyl radical C_6H? *Astron. Astrophys.* **1987**, *175*, L5–L8.

(18) Guélin, M.; Cernicharo, J.; Travers, M.; McCarthy, M.; Gottlieb, C.; Thaddeus, P.; Ohishi, M.; Saito, S.; Yamamoto, S. Detection of a new linear carbon chain radical: C_7H. *Astron. Astrophys.* **1997**, *317*, L1–L4.

(19) Cernicharo, J.; Guélin, M. Discovery of the C_8H radical. *Astron. Astrophys.* **1996**, *309*, L27–L30.

(20) Cernicharo, J.; Guélin, M.; Agúndez, M.; Kawaguchi, K.; McCarthy, M.; Thaddeus, P. Astronomical detection of C_4H^-, the second interstellar anion. *Astron. Astrophys.* **2007**, *467*, L37–L40.

(21) McCarthy, M. C.; Gottlieb, C. A.; Gupta, H.; Thaddeus, P. Laboratory and astronomical identification of the negative molecular ion C_6H^-. *Astrophys. J. Lett.* **2006**, *652*, L141–L144.

(22) Brünken, S.; Gupta, H.; Gottlieb, C. A.; McCarthy, M. C.; Thaddeus, P. Detection of the carbon chain negative ion C_8H^- in TMC-1. *Astrophys. J. Lett.* **2007**, *664*, L43–L46.

(23) Jochnowitz, E. B.; Maier, J. P. Electronic spectra of carbon chains and rings: Astrophysical relevance? *Proc. Int. Astron. Union* **2008**, *4*, 395–402.

(24) Nagarajan, R.; Maier, J. P. Electronic spectra of carbon chains and derivatives. *Int. Rev. Phys. Chem.* **2010**, *29*, 521–554.

(25) Duncan, M. A. Infrared laser spectroscopy of mass-selected carbocations. *J. Phys. Chem. A* **2012**, *116*, 11477–11491.

(26) Zack, L. N.; Maier, J. P. Laboratory spectroscopy of astrophysically relevant carbon species. *Chem. Soc. Rev.* **2014**, *43*, 4602–4614.

(27) Kirkwood, D. A.; Tulej, M.; Pachkov, M. V.; Schnaiter, M.; Güthe, F.; Grutter, M.; Wyss, M.; Maier, J. P.; Fischer, G. Electronic spectra of carbon chain anions: $C_{2n}H^-$ (n=5-12). *J. Chem. Phys.* **1999**, *111*, 9280–9286.

(28) Linnartz, H.; Motylewski, T.; Maier, J. P. The $^2\Pi \leftarrow X^2\Pi$ electronic spectra of C_8H and $C_{10}H$ in the gas phase. *J. Chem. Phys.* **1998**, *109*, 3819–3823.

(29) Taylor, T. R.; Xu, C.; Neumark, D. M. Photoelectron spectra of the $C_{2n}H^-$ (n=1–4) and $C_{2n}D^-$ (n=1–3) anions. *J. Chem. Phys.* **1998**, *108*, 10018–10026.

(30) Garand, E.; Yacovitch, T. I.; Zhou, J.; Sheehan, S. M.; Neumark, D. M. Slow photoelectron velocity-map imaging of the C_nH^- (n=5–9) anions. *Chem. Sci.* **2010**, *1*, 192–201.

(31) Chai, J.-D.; Head-Gordon, M. Long-range corrected hybrid density functionals with damped atom-atom dispersion corrections. *Phys. Chem. Chem. Phys.* **2008**, *10*, 6615.

(32) Riplinger, C.; Neese, F. An efficient and near linear scaling pair natural orbital based local coupled cluster method. *J. Chem. Phys.* **2013**, *138*, 034106.

(33) Guo, Y.; Riplinger, C.; Becker, U.; Liakos, D. G.; Minenkov, Y.; Cavallo, L.; Neese, F. Communication: An improved linear scaling perturbative triples correction for the domain based local pair-natural orbital based singles and doubles coupled cluster method [DLPNO-CCSD (T)]. *J. Chem. Phys.* **2018**, *148*, 011101.

(34) Saitow, M.; Becker, U.; Riplinger, C.; Valeev, E. F.; Neese, F. A new near-linear scaling, efficient and accurate, open-shell domain-based local pair natural orbital coupled cluster singles and doubles theory. *J. Chem. Phys* **2017**, *146*, 164105.

(35) Neese, F. The ORCA program system. *Wiley Interdiscip. Rev.: Comput. Mol. Sci.* **2012**, *2*, 73.

(36) Neese, F. Software update: the ORCA program system, version 4.0. *Wiley Interdiscip. Rev.: Comput. Mol. Sci.* **2018**, *8*, e1327.

(37) Frisch, M. J.; Trucks, G. W.; Schlegel, H. B.; Scuseria, G. E.; Robb, M. A.; Cheeseman, J. R.; Scalmani, G.; Barone, V.; Petersson, G. A.; Nakatsuji, H. et al. Gaussian 16 Revision C.01. 2016; Gaussian Inc. Wallingford CT 2009.

(38) Dunning Jr, T. H. Gaussian basis sets for use in correlated molecular calculations. I. The atoms boron through neon and hydrogen. *J. Chem. Phys.* **1989**, *90*, 1007–1023.

(39) Woon, D. E.; Dunning Jr, T. H. Gaussian basis sets for use in correlated molecular calculations. III. The atoms aluminum through argon. *J. Chem. Phys.* **1993**, *98*, 1358–1371.

(40) Schäfer, A.; Huber, C.; Ahlrichs, R. Fully optimized contracted Gaussian basis sets of triple zeta valence quality for atoms Li to Kr. *J. Chem. Phys.* **1994**, *100*, 5829–5835.

(41) Western, C. M. PGOPHER: A program for simulating rotational, vibrational and electronic spectra. *J. Quant. Spectrosc. Radiat. Transfer* **2017**, *186*, 221–242.

(42) Baryshnikov, G. V.; Valiev, R. R.; Valiulina, L. I.; Kurtsevich, A. E.; Kurtén, T.; Sundholm, D.; Pittelkow, M.; Zhang, J.; Ågren, H. Odd-number cyclo[n]carbons sustaining alternating aromaticity. *J. Phys. Chem. A* **2022**, *126*, 2445–2452.

(43) Karton, A.; Tarnopolsky, A.; Martin, J. M. L. Atomization energies of the carbon clusters C_n (n=2–10) revisited by means of W4 theory as well as density functional, G_n, and CBS methods. *Mol. Phys.* **2009**, *107*, 977–990.

(44) Brémond, E.; Pérez-Jiménez, A.; Adamo, C.; Sancho-Garcia, J.-C. Stability of the polyynic form of C_{18}, C_{22}, C_{26}, and C_{30} nanorings: A challenge tackled by range-separated double-hybrid density functionals. *Phys. Chem. Chem. Phys.* **2022**, *24*, 4515–4525.

(45) Yousaf, K. E.; Taylor, P. R. On the electronic structure of small cyclic carbon clusters. *Chem. Phys.* **2008**, *349*, 58–68.

(46) Neiss, C.; Trushin, E.; Görling, A. The nature of one-dimensional carbon: Polyynic versus cumulenic. *ChemPhysChem* **2014**, *15*, 2497–2502.

(47) Hobbs, L. M.; York, D. G.; Snow, T. P.; Oka, T.; Thorburn, J. A.; Bishof, M.; Friedman, S. D.; McCall, B. J.; Rachford, B.; Sonnentrucker, P. A catalog of diffuse interstellar bands in the spectrum of HD 204827. *Astrophys. J.* **2008**, *680*, 1256.

(48) Hobbs, L. M.; York, D. G.; Thorburn, J. A.; Snow, T. P.; Bishof, M.; Friedman, S. D.; McCall, B. J.; Oka, T.; Rachford, B.; Sonnentrucker, P. et al. Studies of the diffuse interstellar bands. III. HD 183143. *Astrophys. J.* **2009**, *705*, 32.

(49) Zhen, J.; Paardekooper, D.; Candian, A.; Linnartz, H.; Tielens, A. Quadrupole ion trap/time-of-flight photo-fragmentation spectrometry of the hexa-peri-hexabenzocoronene (HBC) cation. *Chem. Phys. Lett.* **2014**, *592*, 211–216.

(50) West, B.; Useli-Bacchitta, F.; Sabbah, H.; Blanchet, V.; Bodi, A.; Mayer, P. M.; Joblin, C. Photodissociation of pyrene cations: Structure and energetics from $C_{16}H_{10}^{+}$ to C_{14}^{+} and almost everything in between. *J. Phys. Chem. A* **2014**, *118*, 7824–7831.

(51) Tielens, A. The molecular universe. *Rev. Mod. Phys.* **2013**, *85*, 1021.

(52) Hrodmarsson, H. R.; Bouwman, J.; Tielens, A. G.; Linnartz, H. Similarities and dissimilarities in the fragmentation of polycyclic aromatic hydrocarbon cations: A case study involving three dibenzopyrene isomers. *Int. J. Mass Spectrom.* **2022**, *476*, 116834.

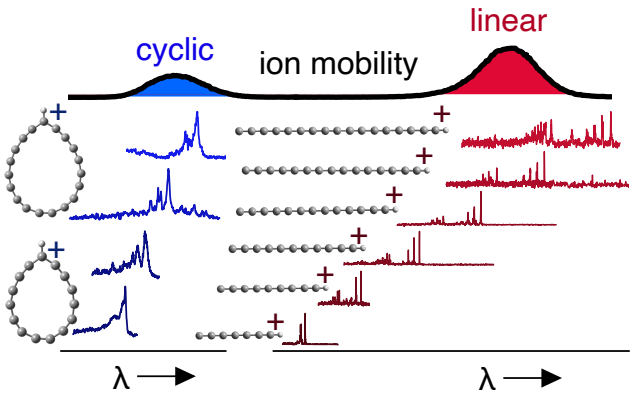

TOC graphic